JOURNAL OF CATALYSIS **173,** 1–9 (1998)
ARTICLE NO. CA971887

# New Catalysts for Hydroprocessing: Bimetallic Oxynitrides $M_I$–$M_{II}$–O–N ($M_I$, $M_{II}$ = Mo, W, V, Nb, Cr, Mn, and Co)

## Part I. Synthesis and Characterization

C. Charles Yu, Sasangan Ramanathan, and S. Ted Oyama[1]

*Laboratory for Environmental Catalysis and Materials, Department of Chemical Engineering, Virginia Tech, Blacksburg, Virginia 24061-0211*

Received August 13, 1996; revised June 24, 1997; accepted September 3, 1997

**A new family of bimetallic oxynitride compounds, $M_I$–$M_{II}$–O–N ($M_I$, $M_{II}$ = Mo, W, V, Nb, Cr, Mn, and Co), has been synthesized by nitriding bimetallic oxide precursors with ammonia gas via a temperature programmed reaction. The oxide precursors are prepared by conventional solid state reaction between two appropriate monometallic oxides. The synthesis involves passing $NH_3$ gas over the oxide precursors at a flow rate of $6.80 \times 10^2$ $\mu$mol $s^{-1}$ (1000 $cm^3$/min) and raising the temperature at a heating rate of $8.3 \times 10^{-2}$ K $s^{-1}$ (5 K/min) to a final temperature ($T_f$) which is held constant for a short period of time ($t_{hold}$). The oxynitrides thus obtained are pyrophoric and need to be passivated before exposing them to air. All these new bimetallic oxynitrides have a face centered cubic crystal structure and high values of surface area. The surface reactivation and the thermal stability of the materials are studied by temperature programmed reduction and this indicates that the compounds can be divided into three groups of different reducibility (high, medium, and low). Their surface activity and surface area are evaluated based on CO chemisorption and $N_2$ physisorption measurements. It is found that the chemisorbed CO number density correlates with the reducibility of the compounds.** 

### INTRODUCTION

Transition metal nitrides are important technological materials. In general they have physical properties characteristic of refractory ceramics, with very high melting points, hardness, and tensile strengths. At the same time, they display electronic and magnetic properties resembling those of metals, such as electrical conductivity, Hall coefficient, magnetic susceptibility, and heat capacity (1, 2). Their extreme hardness and excellent corrosion resistance make them suitable as cutting tools, wear-resistant parts, and hard coatings (3–8). Their metallic properties, sometimes combined with refractory characteristics, make them useful as electronic and magnetic components (9–18) and as superconductors (19–25).

Transition metal nitrides have also received considerable attention as catalysts. There are many studies of their application in ammonia synthesis (26–28), Fischer–Tropsch reaction (29–33), hydrogenation (34–37), oxidation (38, 39), hydrodenitrogenation (HDN) and hydrodesulfurization (HDS) (40–44). Their activities resemble those of the noble Group 8–10 metals (Pt, Pd, Rh, etc.), and in some cases they have superior selectivity, stability, and resistance to poisoning (27, 34, 41–46).

Monometallic nitrides have been investigated extensively since the 1950s and 1960s (1, 47). Studies reveal that their phases can exist over broad composition ranges with appreciable vacancy concentrations and that their physical properties are quite sensitive to composition. Changes in valence electron numbers are probably a major cause of the composition sensitivity. We anticipate that partial exchange of nitrogen by oxygen, and at the same time, partial substitution of one transition metal by another could substantially alter the properties of the compounds.

Compared to the monometallic nitrides, relatively few transition metal bimetallic nitrides have been synthesized and fully characterized (48, 49). It is known that oxygen atoms can substitute for nitrogen atoms in monometallic nitrides due to the similarity in their radius (50, 51). However, the literature on the subject is scarce. No study on the synthesis and characterization of bimetallic oxynitrides of purely transition metals has ever been reported prior to our studies (52–54).

For catalytic applications it is critical for a material to have high specific surface area ($S_g$). Conventional powder metallurgy methods such as direct nitridation of metal powders do not yield high surface area products because of the elevated temperatures necessary for reaction. Nitride powders with very small particle size and high $S_g$ values can be prepared through vapor phase processes. However, such processes produce only very low product yields. In the early 1980s a new preparation method, referred to as temperature programmed reaction, was developed which produces

[1] To whom correspondence should be addressed.



0021-9517/98 $25.00

carbides and nitrides with high specific surface areas (46, 55). In nitride preparation, the method involves placing an oxide precursor in a flowing ammonia stream while raising the temperature in a controlled manner. $\gamma$-$Mo_2N$ with surface area as high as 220 $m^2/g$ has been so prepared (46).

In the current investigation, the temperature programmed reaction technique is applied to bimetallic oxide precursors, prepared by solid state reaction. The bimetallic nitride products are surface active. They all adopt face centered cubic (fcc) crystal structure and have high surface area. In this paper, we will present detailed synthesis procedures and characterization results of these new materials. The catalytic application of these new oxynitrides are reported in a companion paper.

## EXPERIMENTAL

Materials used in the current investigation were molybdenum (VI) oxide ($MoO_3$, 99.95%, Johnson Matthey), tungsten (VI) oxide ($WO_3$, 99.8%, Johnson Matthey), vanadium (V) oxide ($V_2O_5$, 99.9%, Johnson Matthey), niobium (V) oxide ($Nb_2O_5$, 99.9%, Johnson Matthey), chromium (III) oxide ($Cr_2O_3$, 98%, Aldrich), manganese (II, III) oxide ($Mn_3O_4$, Mn 71%, Johnson Matthey), cobalt (II) acetate ($CoC_2H_6O_4 \cdot 4H_2O$, Co 23.6%, Aldrich), and cobalt (II, III) oxide ($Co_3O_4$, Co 72%, Aldrich). The gases employed were $NH_3$ (Linde Anhydrous Grade, 99.99%), He (Linde UHP Grade, 99.999%), CO (Linde Research Grade, 99.97%) and 0.5% $O_2$/He (Linde UHP Grade).

### *Synthesis*

Bimetallic oxide precursors were prepared by the solid state reaction of two monometallic oxides. In all cases one of the oxides was $MoO_3$ or $WO_3$. The two monometallic oxides, at a prechosen metal ratio, were thoroughly intermixed by grinding, pelletized, and fired in air at various final temperatures (Table 1) for 6 h. The temperatures were chosen so that complete reaction of the constituent oxides occurred, as verified by X-ray diffraction. After firing, the solid products were pulverized into fine powders. The bimetallic oxide powders synthesized were individually transferred to a quartz reactor, which was placed inside a tubular resistance furnace, whose temperature was raised at a linear rate of $8.3 \times 10^{-2}$ K $s^{-1}$ (5 K/min) to a final setting ($T_f$) which was held for a period of time ($t_{hold}$). An ammonia gas stream was passed through the oxide powders during the reaction at a flow rate of $6.80 \times 10^2$ $\mu$mol $s^{-1}$ (1000 $cm^3$/min). Table 1 summarizes the synthesis conditions to produce a pure phase for both bimetallic oxides and bimetallic oxynitrides. Each material required different conditions, and these were found by careful variation of the synthesis parameters (time and temperature). After the temperature programmed reaction, the oxynitride samples were passivated at room temperature, using a gas mixture containing 0.5% $O_2$ in He at a flow rate of 24 $\mu$mol $s^{-1}$ (35 $cm^3$/min). The time of passivation was set to 3 h per gram of starting bimetallic oxide used.

### *Characterization*

Both bimetallic oxides and bimetallic oxynitrides was analyzed by X-ray diffraction (XRD), using a Siemens Model D 500 diffractometer with a CuK$\alpha$ monochromatized radiation source for phase identification. The bimetallic oxynitrides were also characterized by inductively coupled plasma (ICP) for elemental composition.

In addition, the oxynitride samples were characterized by a series of measurements consisting of an initial temperature programmed reduction (TPR) to 738 K, CO chemisorption, $N_2$ physisorption, and a final TPR to 1373 K. This sequence was employed to study the reactivation process, to measure the surface activity and surface area, and to evaluate the thermal stability of the compounds under a reductive environment.

**TABLE 1**

**Preparation Conditions for Bimetallic Oxides and Oxynitrides**

| | | | Synthesis of oxides | | Synthesis of oxynitrides | |
|---|---|---|---|---|---|---|
| System ($M_I$–$M_{II}$) | Starting materials | Metal ratio ($M_I$ : $M_{II}$) | Firing temp. ($T_{MAX}$) | Time hold at $T_{MAX}$ | Final temp. ($T_{MAX}$) | Time hold at $T_{MAX}$ ($t_{hold}$) |
| V–Mo | $V_2O_5$–$MoO_3$ | 2 : 1 | 948 K | 6 h | 1037 K | 30 min |
| Nb–Mo | $Nb_2O_5$–$MoO_3$ | 2 : 3 | 1058 K | 6 h | 1063 K | 20 min |
| Cr–Mo | $Cr_2O_3$–$MoO_3$ | 1 : 1 | 1058 K | 6 h | 1013 K | 20 min |
| Mn–Mo | $Mn_3O_4$–$MoO_3$ | 1 : 1 | 1013 K | 6 h | 935 K | 36 min |
| Co–Mo | $CoC_2H_6O_4$–$MoO_3$ | 1 : 1 | 1058 K | 6 h | 892 K | 20 min |
| Nb–W | $Nb_2O_5$–$WO_3$ | 2 : 3 | 1323 K | 6 h | 1113 K | 24 min |
| V–W | $V_2O_5$–$WO_3$ | 1 : 1 | 1323 K | 6 h | 1009 K | 110 min |
| Mo–W | $MoO_3$–$WO_3$ | 1 : 1 | 1058 K | 6 h | 991 K | 20 min |
| Co–W | $Co_3O_4$–$WO_3$ | 1 : 1 | 1370 K | 6 h | 1063 K | 24 min |

Approximately 0.2 g bimetallic oxynitride samples were loaded into a quartz microreactor, which was then placed inside the tubular resistance furnace. A 10% $H_2$ in He gas mixture was passed through the sample at a rate of 20 $\mu$mol $s^{-1}$ (30 $cm^3$/min). The temperature was increased at a linear rate of 0.16 K $s^{-1}$ (10 K/min) to 738 K, where it was held for 2 h. The temperature of the sample was measured through a chromel–alumel thermocouple placed in the center of the reactor bed. During the TPR process, the effluent gas stream was sampled into a mass spectrometer (Ametek/Dycor Model MA100) chamber through a variable leak valve (Granville Phillips Model 203). A computer (Thoroughbred, 80386SX-16) recorded the mass signals of the effluent gas and the sample temperatures through a RS232 interface. At the end of the TPR process, the $H_2$/He gas mixture was switched to pure He, and the samples were brought to room temperature for CO chemisorption measurements.

CO chemisorption was used to titrate the surface metal atoms in the sample. After the 2-h reduction described above, pulses of CO gas were introduced through a sampling valve with the He carrier gas stream passing over the samples. The total uptake was calculated by referring the areas under the CO mass signal (28) peaks to the known quantity of 12 $\mu$mol CO for a single peak.

Surface areas were determined immediately after the CO uptake measurements by a similar flow technique using a 30% $N_2$ in He gas mixture passed over the samples maintained at liquid nitrogen temperature. The amount of physisorbed $N_2$ was obtained by comparing the area of the desorption peaks to the area of calibrated $N_2$ pulses containing 38 $\mu$mol $N_2$/pulse. The surface area was then calculated from the single point BET equation.

The final TPR to 1373 K was carried out, in the same manner as the initial TPR, on the same samples which had undergone CO chemisorption. During the TPR process, the mass signals of the effluent gases as well as the sample temperature were again recorded.

## RESULTS

Figures 1a–i are the XRD patterns of the bimetallic oxides prepared by solid state reaction. The prominent features of each product's XRD pattern, i.e. peak position and intensity, do not match those of the parent oxides, nor their reduced forms. The results suggest that at least the major phases of the products are true bimetallic oxides, instead of mechanical mixtures of the starting oxides. The XRD patterns of bimetallic oxynitrides, prepared by temperature programmed reaction, are shown in Figs. 2a–i. The results indicate, interestingly, that all the oxynitrides thus synthesized have a face-centered cubic (fcc) metallic arrangement. The XRD peak d-spacings and their indexing are listed in Table 2. Furthermore, the broadening of the XRD peaks

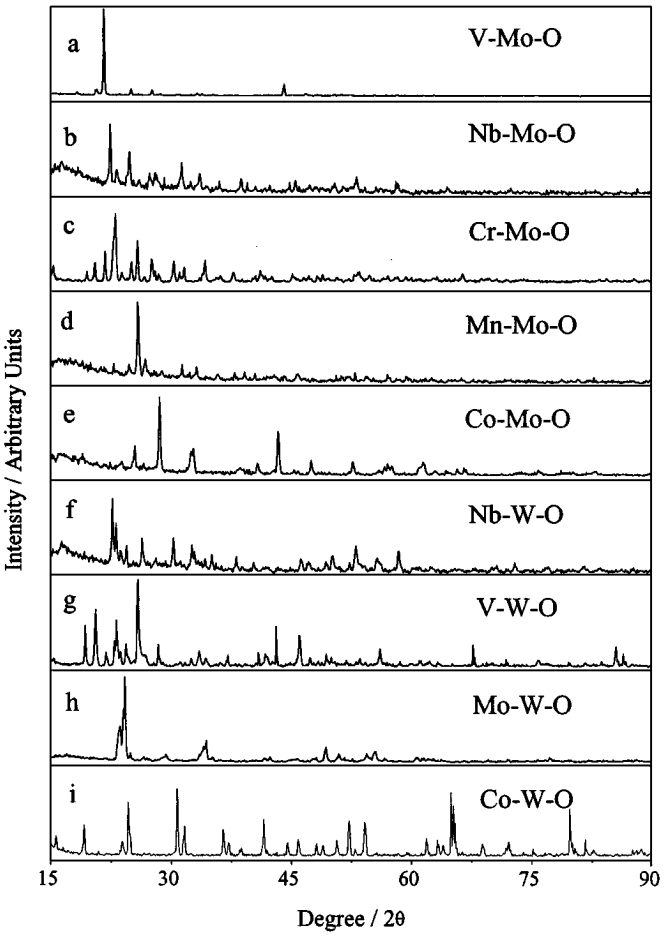


**FIG. 1.** XRD patterns of bimetallic oxides.

indicates that these oxynitrides have very small crystallite sizes, which in turn suggests high surface areas in these materials. The elemental analysis results are presented in Table 3.

Table 4 summarizes the CO uptakes, surface areas, and the active site density of the oxynitrides, together with their

**TABLE 2**

**XRD Peak d-Spacing and Indexing of Bimetallic Oxynitrides**

| Indexing | (111) | (200) | (220) | (311) | (222) | |
|---|---|---|---|---|---|---|
| Compounds | d-spacing/nm | | | | | $a_o$/nm |
| V–Mo–O–N | 0.238 | 0.206 | 0.146 | 0.124 | 0.119 | 0.413 |
| Nb–Mo–O–N | 0.245 | 0.211 | 0.150 | 0.127 | 0.122 | 0.423 |
| Cr–Mo–O–N | 0.238 | 0.206 | 0.146 | 0.125 | 0.119 | 0.413 |
| Mn–Mo–O–N | 0.252 | 0.218 | 0.154 | — | — | 0.436 |
| Co–Mo–O–N | 0.243 | 0.210 | 0.149 | — | — | 0.420 |
| Nb–W–O–N | 0.241 | 0.209 | 0.148 | 0.126 | — | 0.418 |
| V–W–O–N | 0.239 | 0.206 | 0.146 | 0.125 | 0.120 | 0.414 |
| Mo–W–O–N | 0.240 | 0.207 | 0.147 | 0.125 | — | 0.416 |
| Co–W–O–N | 0.240 | 0.205 | 0.146 | 0.125 | — | 0.413 |

**TABLE 3**

**Molar Composition of Bimetallic Oxynitride $M^{I}_{W}M^{II}_{x}O_yN_z$ (from Elemental Analysis)**

| Sample | $M^I:M^{II}$ (theoretical) | V | Nb | Cr | Mn | Co | Mo | W | O | N |
|---|---|---|---|---|---|---|---|---|---|---|
| V–Mo–O–N | 2:1 | 2.0 | | | | | 1.0 | | 1.7 | 2.4 |
| Nb–Mo–O–N | 2:3 | | 2.0 | | | | 2.6 | | 3.0 | 4.2 |
| Cr–Mo–O–N | 1:1 | | | 1.0 | | | 1.3 | | 2.3 | 1.4 |
| Mn–Mo–O–N | 1:1 | | | | 1.0 | | 1.0 | | 1.5 | 0.88 |
| Co–Mo–O–N | 1:1 | | | | | 1.0 | 1.0 | | 1.6 | 0.79 |
| Nb–W–O–N | 2:3 | | 2.0 | | | | | 2.8 | 4.6 | 5.1 |
| V–W–O–N | 1:1 | 1.0 | | | | | | 1.4 | 2.7 | 2.5 |
| Mo–W–O–N | 1:1 | | | | | | 1.0 | 1.0 | 2.4 | 2.1 |
| Co–W–O–N | 1:1 | | | | | 1.0 | | 1.0 | 1.2 | 1.0 |

crystallite size and particle size. The crystallite size ($D_c$) was calculated by the Scherrer equation (56), based on XRD peak broadening. The particle size ($D_p$) was calculated from the equation: $D_p = 6/[S_g\rho]$ (57), where $\rho$ is taken to be 10.2 g cm$^{-3}$ for Mo oxynitride compounds and 18.9 g cm$^{-3}$ for W oxynitride compounds, assuming perfect rock salt structures for these compounds.

Figures 3a–i are the TPR traces and the temperature profiles of the oxynitride surface reactivation process. The mass signal 15 represents ammonia, while signals 18 and 28 represent water and nitrogen, respectively. It is interesting to notice that, in all cases, the nitrogen peak appears earlier than the ammonia peak. Generally, the nitrogen traces have more features, showing a number of peaks. The water peak always comes up the latest.

Figures 4a–i are the TPR traces of masses 12, 14, 16, 18, and 44 versus temperature for the samples exposed to CO. The heating rate was 0.17 K s$^{-1}$ (10 K/min) in all cases. The signals at 12, 14, 18, and 44 represent carbon monoxide, nitrogen, water, and carbon dioxide, respectively, while the signal at 16 can be attributed to both ammonia and methane. The TPR process of the CO adsorbed samples can be roughly divided into three regions: (1) the low temperature desorption region (room temperature up to 700 K), where the adsorbed CO comes off the sample surface in the forms of CO, $CO_2$, or $CH_4$; (2) the middle temperature

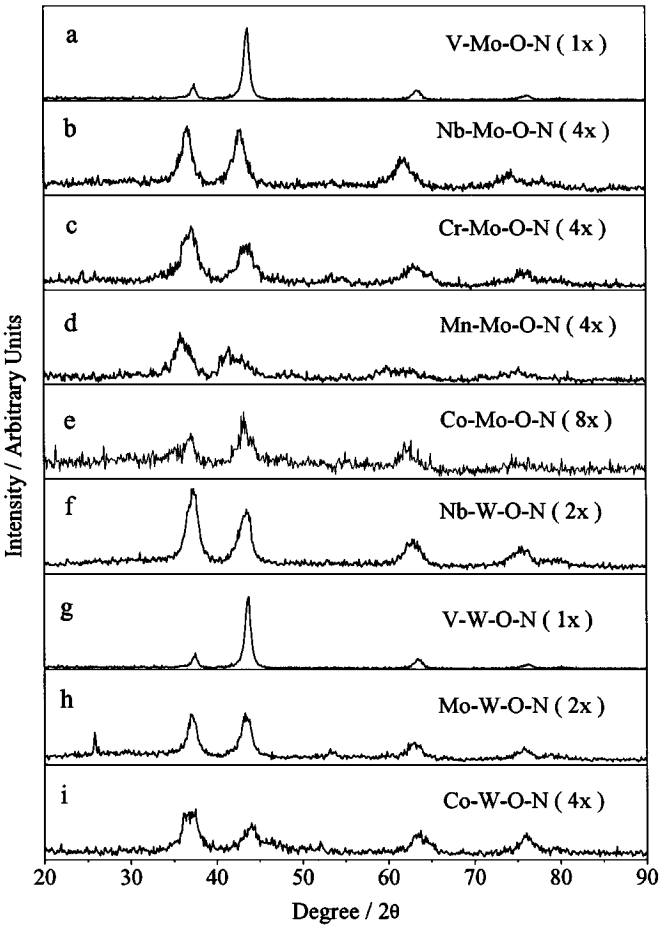


**FIG. 2.** XRD patterns of bimetallic oxynitrides.

**TABLE 4**

**Characteristics of Bimetallic Oxynitrides**

| Compounds | Reducibility (from TPR) | CO uptake ($\mu$mol g$^{-1}$) | Surface area ($S_g$ m$^2$ g$^{-1}$) | Site density ($\times 10^{15}$ cm$^{-2}$) | | Particle size $D_p$ (nm) | Crystallite size $D_c$ (nm) |
|---|---|---|---|---|---|---|---|
| V–Mo–O–N | High | 167 | 74 | 0.14 | H | 7.9 | 11 |
| Cr–Mo–O–N | High | 163 | 90 | 0.11 | H | 6.6 | 3.9 |
| Co–Mo–O–N | High | 186 | 103 | 0.11 | H | 5.7 | 4.5 |
| Mo–W–O–N | Mod | 59.8 | 118 | 0.031 | M | 5.0 | 6.5 |
| Nb–W–O–N | Mod | 32.7 | 81 | 0.024 | M | 3.9 | 5.2 |
| Co–W–O–N | Mod | 12.5 | 45 | 0.017 | M | 7.1 | 3.8 |
| Mn–Mo–O–N | Mod | 10.6 | 37 | 0.017 | M | 15.8 | 3.5 |
| V–W–O–N | Low | 9.67 | 62 | 0.0094 | L | 5.1 | 6.7 |
| Nb–Mo–O–N | Low | 11.2 | 121 | 0.0056 | L | 4.9 | 5.3 |

*Note.* $D_p = 6/S_g\rho$; $\rho_{Mo} = 10.2$ g cm$^{-3}$; $\rho_W = 18.9$ g cm$^{-3}$; $D_c = K\lambda/\beta \cos\theta$; $\beta^2 = B^2 - b^2 = B^2 - 0.1^2$; H = High; M = Mod; L = Low.

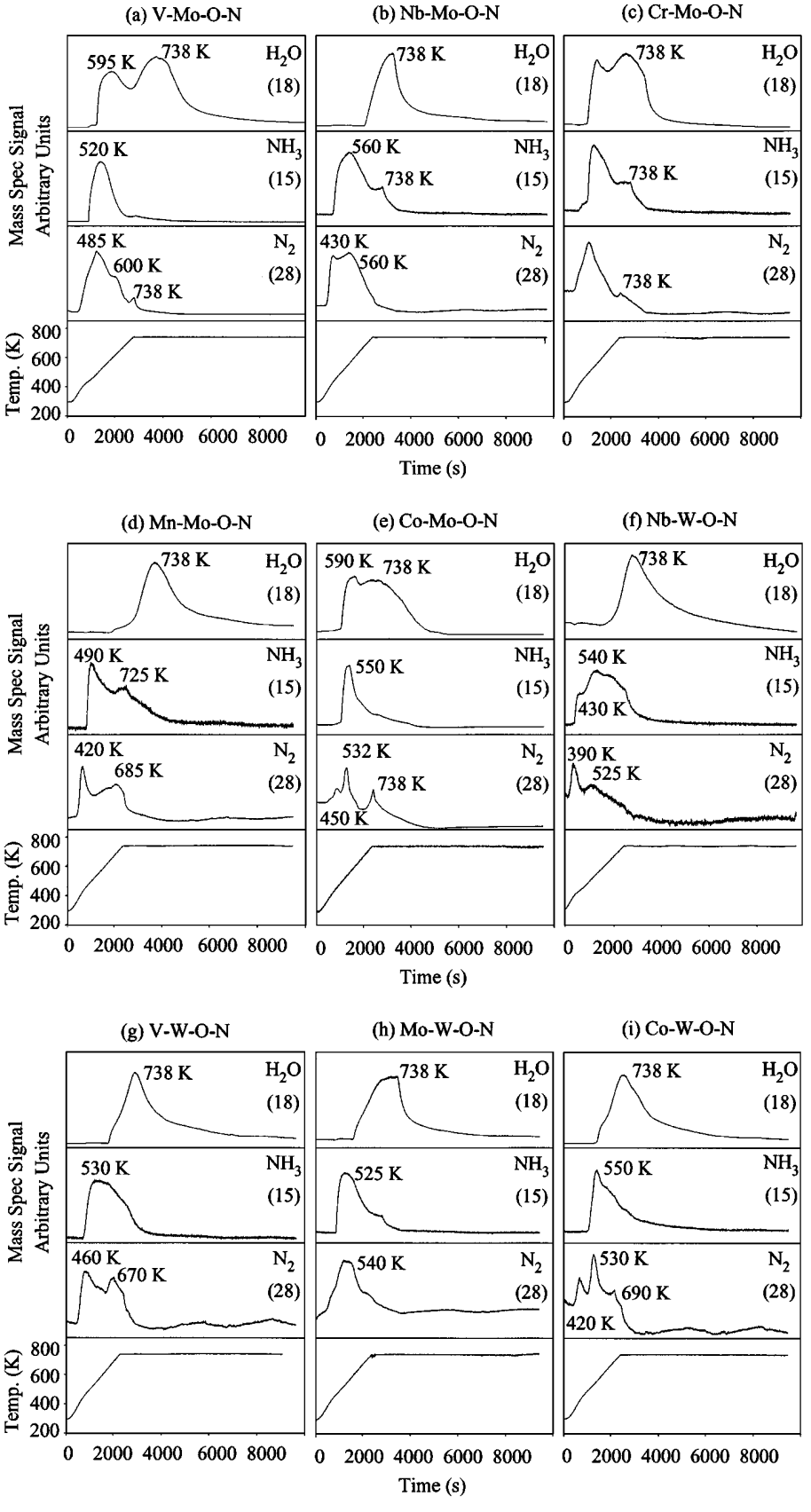


**FIG. 3.** TPR traces and temperature profiles of oxynitride surface reactivation.

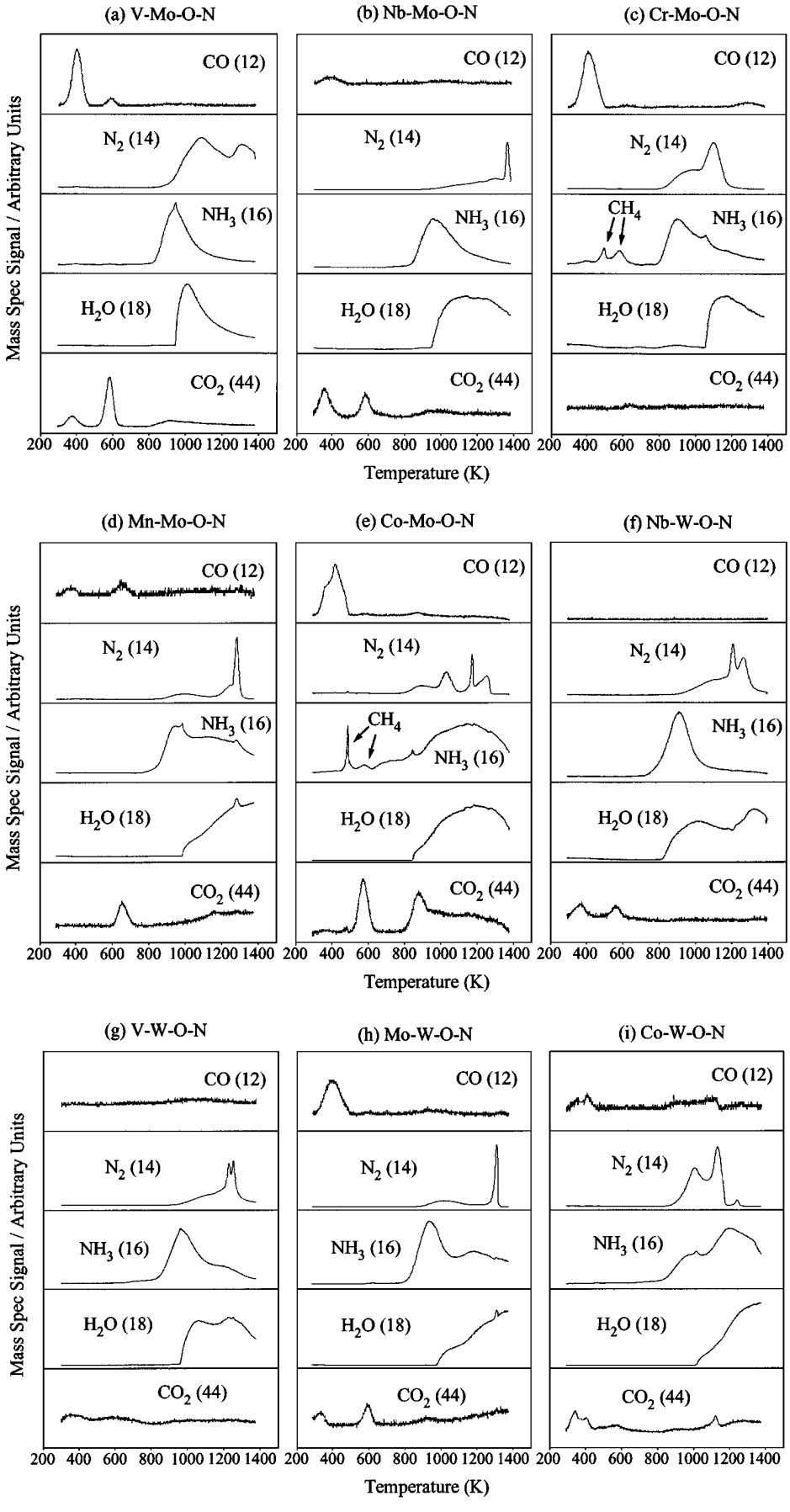


**FIG. 4.** TPR traces of oxynitride sample after CO adsorption.

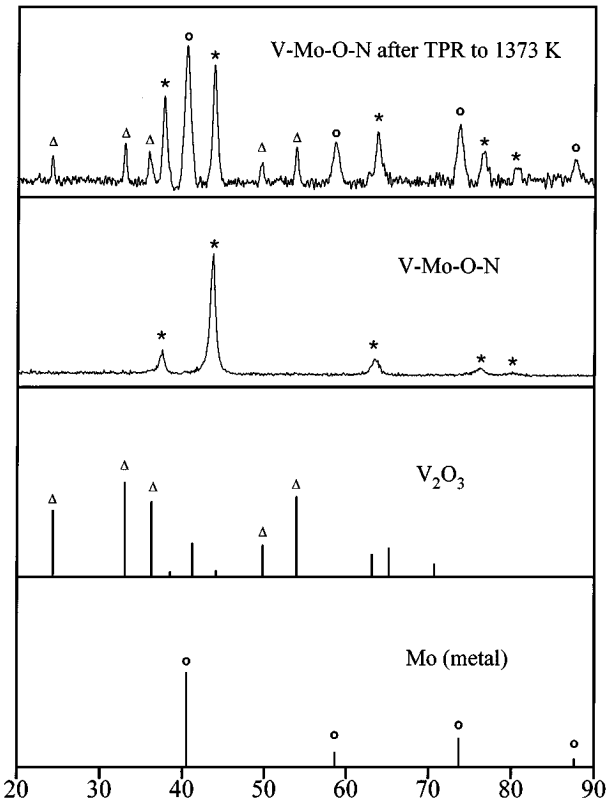


**FIG. 5.** XRD patterns of (a) V–Mo–O–N after TPR to 1373 K, (b) V–Mo–O–N, (c) $V_2O_3$, and (d) Mo metal.

reduction region (700 K to 1050 K), where the oxynitrides are reduced by hydrogen as indicated by the formation of ammonia and water; (3) the high temperature destruction region (above 1050 K), where the final decomposition of the sample starts to occur. This is indicated by the high intensity nitrogen signals (in most cases appearing as sharp peaks), as well as the high intensity water signals. As an example, the XRD analysis of V–Mo–O–N after heating to 1373 K in $H_2$ shows mostly metallic Mo, some remnant V–Mo–O–N phase, and a small amount of $V_2O_3$ (Fig. 5).

## DISCUSSION

All the oxynitrides reported here have a similar five-peak XRD pattern (four are visible in the scale presented), which is consistent with a rock salt crystal structure (B1 structure space group *Fm3m*), where the metal atoms are found in a face-centered cubic (fcc) arrangement and N or O fill every octahedral interstitial position (58). For bimetallic nitrides this type of structure is unreported, as indicated in a recent comprehensive review (59), and the compounds may be considered to constitute a new class of materials. Comparison of the bimetallic compounds to the monometallic compounds shows considerable differences. $Mo_2N$ and $W_2N$ have the $L'_3$ structure with a face-centered cubic metallic lattice but with N filling only half of the available octahedral holes (60). $Cr_2N$ has a hexagonal closed packed (hcp) structure, $Mn_4N$ has a perovskite structure, and $Co_2N$ has an orthorhombic structure (61). Only VN and NbN have the rock-salt structure. It is highly unlikely that the bimetallic compounds are physical mixtures of the monometallic compounds. First, all of the members of the series give the same XRD pattern, irrespective of the constituents. A careful study of the V–Mo–O–N system reveals that the temperature-programmed reduction of the mixed compounds is different from those of the pure $Mo_2N$ and VN phases (62), suggesting that the V–Mo oxynitride is a true compound. Furthermore, near edge X-ray absorption fine structure (NEXAFS) studies of the Nb–Mo and V–Mo (63, 64) systems show that the electronic structure of the mixed compounds is unique and not a superposition of the single compounds. The results are consistent with the metallic components being thoroughly intermixed in a random solution manner.

The elemental analysis results (Table 2) confirm the presence of both transition metals close to the ratios expected from the initial oxide compositions. The slight deviations observed (Nb–Mo, Cr–Mo, Nb–W, V–W) occur with the highest synthesis temperatures and are consistent with volatilization of the lower melting point oxide.

The elemental analysis results also show a substantial excess of the nonmetallic components (O, N) over that expected for the rock-salt structure. Part of the discrepancy is due to the inherent nature of these interstitial compounds to form considerable metal vacancies, depending on the preparation or heat treatment conditions. Actually both metal and nonmetal vacancies are common. For example, titanium oxide is found with compositions ranging from $TiO_{0.64}$ (36% O vacancies) to $TiO_{1.26}$ (21% Ti vacancies) (61). Similarly, titanium nitride exists in a range from $TiN_{0.42}$ (58% N vacancies) to $TiN_{1.16}$ (14% Ti vacancies) (47). However, in the case of the present compounds, it is likely that the nonstoichiometry as manifested by excess oxygen is also due to the presence of a thin surface oxide layer from the passivation process. Because of the small crystallite size of the materials, to be discussed later, the surface contribution is substantial and can amount to at least 25% of the atomic composition. This can be estimated (Fig. 6) simply by taking a typical crystallite in the shape of a cube of 5-nm side dimension (Table 4). Since the typical fcc conventional unit cell is approximately 0.4 nm in size (Table 2), this places $5/0.4 = 12$ unit cells per edge, or $12 \times 12$ per face and $12 \times 12 \times 12$ per volume. Since an fcc unit cell has four atoms in total and two on each face, the total atoms in the crystallite is $4 \times 12 \times 12 \times 12$, while the total atoms on the surface is $2 \times 6 \times 12 \times 12$. This gives a surface to volume atomic ratio of 1 : 4 or 25%.

The initial temperature-programmed reduction to 738 K in 10% $H_2$/He sequentially produces $N_2$, $NH_3$, and $H_2O$. The

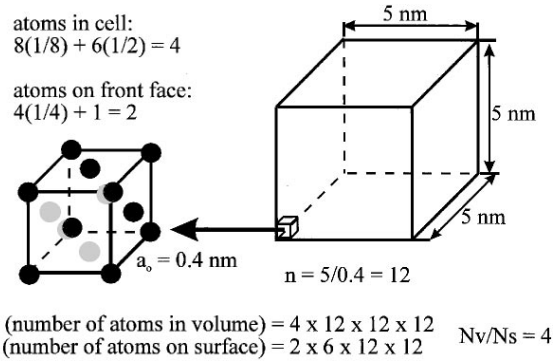


**FIG. 6.** Calculation of surface to volume ratio in a 5 nm cubic crystallite.

treatment is evidently reducing the surface. The appearance of $N_2$ and $NH_3$ before $H_2O$ suggests that oxygen is held more tightly than nitrogen. The samples can be categorized according to the peak shapes of the $H_2O$ production traces. For a first group of compounds, V–Mo–O–N, Cr–Mo–O–N, and Co–Mo–O–N, $H_2O$ appears in two peaks, one at a lower temperature and the other at a higher temperature (the V–Mo–O–N shows a smaller low-temperature feature). For a second group of samples, Mn–Mo–O–N, Nb–W–O–N, Mo–W–O–N, and Co–W–O–N, $H_2O$ is in the form of broad peaks that appear just as the temperature program reaches its maximum of 738 K. Finally, for a third group of compounds, Nb–Mo–O–N and V–W–O–N, the $H_2O$ peaks are relatively narrow and appear after the longest reduction times. Clearly, the ease of reduction is decreasing in going from the first group to the last. This has been indicated in column 2 of Table 4. Examination of the elements comprising the three groups shows that, in general, the order of reducibility is Mo > W and V > Nb. In essence this follows the trend for transition metals, first row > second row > third row.

CO chemisorption can be used to titrate accessible surface metal atoms in the materials (63, 64). The CO uptakes of the current samples range from low (9.67 $\mu$mol $g^{-1}$) to moderate (186 $\mu$mol $g^{-1}$). Normally for metals and metal alloys the surface site density is $\sim 1 \times 10^{15}$ $cm^{-2}$ (65). The values obtained in this study are in the range 0.01–0.10 $\times$ $10^{15}$ $cm^{-2}$, indicating 1–10% of the metal atoms are chemisorbing CO. These values are consistent with previously reported quantities for carbides and nitrides (62, 65). It is likely that the initial 2-h reduction to 738 K is not able to remove all the N and O species from the surface which block CO chemisorption (67). This may be partially the case because N and O can be replenished from the bulk. These species are known to be mobile in the subsurface at these temperatures (37). The amount of CO chemisorbed on the oxynitride surface is found to track closely with the surface reducibility of the compounds (Table 4, column 5). This is reasonable, since more chemisorption sites are likely to be opened up for the more reducible compounds.

The unusually broad XRD peaks indicate finely divided substances, which in turn suggest high surface area. This is confirmed by the results that all the oxynitride samples obtained in this study have high surface area, from 37 $m^2 g^{-1}$ up to 121 $m^2 g^{-1}$. Moreover, the crystallite size ($D_c$), calculated by the Scherrer equation (56) based on XRD peak broadening, indicates dimensions of the order 3 to 11 nm. The particle size ($D_p$), calculated from the surface area of the material (57), indicates dimensions of the order 4 to 16 nm. Thus, there is good agreement between $D_p$ and $D_c$.

The final temperature-programmed reduction to 1373 K shows decomposition of the compounds at temperatures well above those used in the reactivation pretreatment. This indicates that the samples are stable to reduction at moderate conditions. Those conditions are the ones encountered during actual application.

## CONCLUSIONS

A new catalyst series, $M_I$–$M_{II}$–O–N ($M_I$, $M_{II}$ = Mo, W, V, Nb, Cr, Mn, and Co), has been prepared by a temperature-programmed reaction process. The temperatures required for the synthesis are moderate (<1120 K), the cycles are short (moderate heating rate and holding times), and the parameters are easy to control. The oxide precursors used for making these oxynitrides are prepared by conventional solid state reaction using common starting materials.

All the oxynitrides synthesized have face centered cubic (fcc) structure and high surface area (37–121 $m^2$/g). The CO uptakes of the samples range from low (9.67 $\mu$mol $g^{-1}$) to moderate (186 $\mu$mol $g^{-1}$). The amount of CO chemisorbed is found to relate closely with the surface reducibility of the compounds. The high temperature TPR measurements indicate that the compounds are stable at moderate temperature in reductive environments. Their active surface combined with high surface area make these new materials very interesting candidates as catalysts.

## ACKNOWLEDGMENTS

We thank Dr. Fawzy Sherif for help with the elemental analysis. Funding for this work from the Department of Energy, Office of Basic Energy Sciences, Grant DE-FG02-96ER14669, the DOE Advanced Coal Research at U.S. Universities Program, Grant DE-FG26-97FT97265, and Akzo Nobel is greatly appreciated.

## REFERENCES

1. Toth, L. E., "Transition Metal Carbides and Nitrides," New York, Academic Press, 1971.
2. Oyama, S. T., "The Chemistry of Transition Metal Carbides and Nitrides," Blackie Academic & Professional, London, 1996.
3. Schwartzkopf, P., and Kieffer, R., *in* "Refractory Hard Metals," MacMillan, New York, 1953.
4. Samsonov, G. V., *in* "Refractory Transition Metal Compounds; High Temperature Cermets," Academic Press, New York/London, 1964.

5. Molarius, M., Korhonen, A. S., and Ristolainen, E. O., *J. Vac. Sci. Technol. A* **3**, 2419 (1985).
6. DiSalvo, F. J., *Science* **247**, 649 (1990).
7. Fix, R. M., Gordon, R. G., and Hoffman, D. M., *Chem. Mater.* **2**, 235 (1990).
8. Dressler, S., *Indus. Heating*, **October**, 38 (1992).
9. Wilner, G. W., and Berger, J. A., *J. Met.* **7**, 360 (1955).
10. Mekata, M., *J. Phys. Soc. Jpn.* **17**, 796 (1962).
11. Tim, T. K., and Takahashi, M., *Appl. Phys. Lett.* **20**, 492 (1972).
12. Tagawa, K., Kita, E., and Tasaki, A., *Jpn. J. Appl. Phys.* **21**, 1596 (1982).
13. Garceau, W. J., and Herb, G. K., *Thin Solid Films* **60**, 237 (1979).
14. Ernsberger, C., Miller, A., and Banks, D., *J. Vac. Sci. Technol. A* **3**, 2303 (1985).
15. Wittmer, M., and Melchior, H., *Thin Solid Films* **93**, 397 (1982).
16. Wittmer, M., *J. Vac. Sci. Technol. A* **3**, 1979 (1985).
17. Kumar, N., McGinn, J. T., Pourrezaei, K., Lee, B., and Douglas, C., *J. Vac. Sci. Technol. A* **6**, 1602 (1988).
18. Otani, Y., Hurley, D. P. F., Sun, H., and Coey, J. M. D., *J. Appl. Phys.* **69**, 5584 (1991).
19. Storms, E. K., *LAMS-2674* (Part II) (1962).
20. Courtney, T. H., Reintjes, J., and Wulff, J., *J. Appl. Phys.* **36**, 660 (1965).
21. Toth, L. E., Wang, C. P., and Yen, C. M., *Acta Met.* **14**, 1403 (1966).
22. Shy, Y. M., Toth, L. E., and Somasundaram, R., *J. Appl. Phys.* **44**, 5539 (1973).
23. Toth, L. E., and Yen, C. M., *J. Phys. Chem. Solids* **27**, 1815 (1966).
24. Yen, C. M., Toth, L. E., and Shy, Y. M., *J. Appl. Phys.* **38**, 2268 (1967).
25. Bell, H., Shy, Y. M., Anderson, D. E., and Toth, L. E., *J. Appl. Phys.* **39**, 2797 (1968).
26. Aika, K., and Ozaki, A., *J. Catal.* **14**, 311 (1969).
27. Boudart, M., Oyama, S. T., and Leclercq, L., *in* "Proc. 7th Int. Cong. Catal. Tokyo, 1980" (T. Seiyama and K. Tanabe, Eds.), Vol. 1, p. 578. Kodansha, Tokyo, 1980.
28. Volpe, L., and Boudart, M., *J. Phys. Chem.* **90**, 4874 (1986).
29. Anderson, R. B., Shultz, J. F., Seligman, B., Hall, W. K., and Storch, H. H., *J. Am. Chem. Soc.* **72**, 3502 (1950).
30. Hall, W. K. E., Dieter, W., Hofer, L. J. E., and Anderson, R. B., *J. Am. Chem. Soc.* **75**, 1442 (1953).
31. Anderson, R. B., *Catal. Rev.-Sci. Eng.* **21**(1), 53 (1980).
32. Yeh, E. B., Jaggi, N., Butt, J. B., and Schwartz, L. H., *J. Catal.* **91**, 231 (1985).
33. Yeh, E. B., Schwartz, L. H., and Butt, J. B., *J. Catal.* **91**, 241 (1985).
34. Saito, M., and Anderson, R. B., *J. Catal.* **63**, 438 (1980).
35. Saito, M., and Anderson, R. B., *J. Catal.* **67**, 296 (1981).
36. Ranhotra, G. S., Haddix, G. W., Bell, A. T., and Reimer, J. A., *J. Catal.* **108**, 24 (1987).
37. Ranhotra, G. S., Bell, A. T., and Reimer, J. A., *J. Catal.* **108**, 40 (1987).
38. Kharlamov, A. I., and Kirillova, N. V., *React. Kinet. Catal. Lett.* **14**, 141 (1980).
39. Kharlamov, A. I., and Kirillova, N. V., *React. Kinet. Catal. Lett.* **15**, 345 (1980).
40. Schlatter, J. C., Oyama, S. T., Metcalfe, J. E., III, and Lambert, J. M., Jr., *Ind. Eng. Chem. Res.* **27**, 1648 (1988).
41. Sajkowski, D. J., and Oyama, S. T., preprints, Petroleum Chemistry Division, Symposium, "The Chemistry of W/Mo Catalysis, 199th ACS National Meeting, Boston, MA, April 22–27, 1990."
42. Markel, E. J., and Van Zee, J. W., *J. Catal.* **126**, 643 (1990).
43. Ramanathan, S., and Oyama, S. T., *J. Phys. Chem.* **99**, 16365 (1995).
44. Sajkowski, D. J., and Oyama, S. T., *Appl. Catal. A* **134**, 339 (1996).
45. Oyama, S. T., and Haller, G. L., *Catalysis, Spec. Period. Rep.* **5**, 333 (1981).
46. Volpe, L., and Boudart, M., *J. Solid State Chem.* **59**, 332 (1985).
47. Juza, R., *in* "Advances in Inorganic Chemistry and Radiochemistry" (H. J. Emeleus and A. G. Sharpe, Eds.), Vol. 9, p. 81. Academic Press, New York and London, 1966.
48. Bem, D. S., and Zur Loye, H. C., *J. Solid State Chem.* **104**, 467 (1993).
49. Yamamoto, T., Kikkawa, S., and Kanamaru, F., *Solid State Ionics* **148**, 63 (1993).
50. Kiessling, R., and Peterson, L., *Acta Met.* **2**, 675 (1954).
51. Schönberg, N., *Acta Chem. Scand.* **8**, 208 (1954).
52. Yu, C. C., and Oyama, S. T., *J. Solid St. Chem.* **116**, 205 (1995).
53. Yu, C. C., and Oyama, S. T., *J. Mater. Sci.* **30**, 4037 (1995).
54. Yu, C. C., Ramanathan, S., Sherif, F., and Oyama, S. T., *J. Phys. Chem.* **98**, 13038 (1994).
55. Oyama, S. T., Ph.D. dissertation, Stanford University, 1981.
56. Scherrer, P., *Gött. Nachr.* **2**, 98 (1918).
57. Smith, J. M., "Chemical Engineering Kinetics," 3rd ed., p. 328. McGraw–Hill, New York, 1981.
58. Hyde, B. G., and Anderson, S., "Inorganic Crystal Structures," Wiley, New York, 1989.
59. Brese, N. E., and O'Keeffe, M., Complexes, clusters and crystal chemistry, *in* "Structure and Bonding," Vol. 79, p. 307. Springer-Verlag, Berlin, 1992.
60. Oyama, S. T., *J. Solid State Chem.* **96**, 442 (1992).
61. Juza, R., and Sachsze, S., *Z. Anorg. Chem.* **253**, 95 (1945).
62. Yu, C. C., Ramanathan, S., Dhandapani, B., Chen, J. G., and Oyama, S. T., *J. Phys. Chem. B* **101**, 512 (1997).
63. Kapoor, R., Oyama, S. T., and Chen, J. G., *J. Phys. Chem. B* **101**, 1543 (1997).
64. Lee, J. S., Locatelli, S., Oyama, S. T., and Boudart, M., *J. Catal.* **125**, 157 (1990).
65. Lee, J. S., Lee, K. H., and Lee, J. Y., *J. Phys. Chem.* **96**, 362 (1992).
66. Foger, K., Dispersed metal catalysts *in* "Catalysis, Science and Technology" (L. R. Anderson and M. Boudart, Eds.), Vol. 6, p. 227. Springer-Verlag, Berlin, 1984.
67. Oyama, S. T., Schlatter, J. C., Metcalfe, J. E., III, and Lambert, J. M., Jr., *Ind. Eng. Chem. Res.* **27**, 1639 (1988).
68. Ko, E. I., and Madix, R. J., *Surf. Sci.* **100**, L505 (1980).
69. Ko, E. I., and Madix, R. J., *Surf. Sci.* **109**, 221 (1981).
70. Leary, K. J., Michaels, J. N., and Stacy, A. M., *J. Catal.* **101**, 301 (1986).